

Controlled CVD growth of highly <111>-oriented 3C-SiC

Jing-Jia Huang^{a,b}, Christian Militzer^{a,b}, Charles Wijayawardhana^b, Urban Forsberg^a, Lars Ojamäe^a, Henrik Pedersen^{a*}

^a *Department of Physics, Chemistry and Biology, Linköping University, SE-581 83 Linköping, Sweden*

^b *SGL Carbon GmbH, Drachenburgstraße 1, DE-53170 Bonn, Germany*

* Corresponding author: henrik.pedersen@liu.se

Abstract

Highly <111>-oriented 3C-SiC coatings with distinct surface morphology consisting of hexagonally shaped pyramidal crystals were prepared by chemical vapor deposition (CVD) using silicon tetrachloride (SiCl₄) and toluene (C₇H₈) at $T \leq 1250$ °C and $p = 10$ kPa. In contrast, similar deposition conditions, using methane (CH₄) as carbon precursor, resulted in randomly oriented 3C-SiC coatings with a cauliflower-like surface of SiC crystallites. No excess carbon was detected in the highly <111>-oriented 3C-SiC samples despite the use of aromatic hydrocarbons. The difference in the preferred growth orientation of the 3C-SiC coatings deposited using C₇H₈ and CH₄ as carbon precursors is explained via quantum chemical calculations of binding energies on various crystal planes. The adsorption energy of C₆H₆ on the SiC (111) plane was 6 times higher than that on the (110) surface. On the other hand, the CH₃ exhibited equally strong adsorption on both planes. This suggests that the highly <111>-oriented 3C-SiC growth in the C₇H₈ process, where both C₆H₆ and CH₃ are considered the main active carbon-containing film forming species, is due to the highly preferred adsorption on (111) planes, while the lower surface energy of the (110) plane controls the growth orientation in the CH₄ process, in which only CH₃ contributes to the film deposition.

INTRODUCTION

Polycrystalline silicon carbide (SiC) is a protective coating of choice in many industries due to its high chemical inertia, hardness and temperature stability. Among SiC polytypes, cubic SiC, also known as 3C- or β -SiC, is the most used in refractory applications due to its relatively low formation temperature. One of the techniques frequently adopted for the synthesis of polycrystalline 3C-SiC is chemical vapor deposition (CVD)¹. In a SiC CVD process, multicomponent precursors, e.g. methyl trichlorosilane, can assure unity of C/Si ratio in the gas phase, whereas single-component precursors containing only C or Si can grant the process extra degrees of freedom in choosing different Si- and C-source precursors². Chlorinated silanes, especially silicon tetrachloride (SiCl_4) are widely used precursors in many SiC processes. The addition of Cl to the SiC CVD processes has been reported to not only increase the growth rate but also prevent the formation of Si droplets in the gas phase. The stronger Si-Cl bonds (400 kJ/mol)³ can suppress the formation of weaker Si-Si bonds (226 kJ/mol)^{3,4}. In terms of the C-source precursor, branched and small hydrocarbons such as ethylene or propane are often used since they can produce high-quality SiC coatings and are available at high purities.

As in many polycrystalline materials, the physical and chemical properties of 3C-SiC coatings are dependent on the crystalline orientation. It has been shown that the Vickers microhardness of $\langle 111 \rangle$ -oriented 3C-SiC films, i.e. films in which the (111) planes were aligned parallel to the surface, was higher than those $\langle 110 \rangle$ -oriented⁵. The (110) and (111) planes are the two planes in 3C-SiC with the lowest surface energy; 3.4 J/m² and 4.2 J/m², respectively⁶. In the SiCl_4 -based 3C-SiC CVD processes, the preferred growth orientation of resultant coatings varies with the selection of hydrocarbons as well as the deposition conditions. It was reported that using CH_4 as carbon source, highly $\langle 111 \rangle$ -oriented 3C-SiC can be produced either at $T = 1200^\circ\text{C}$, $p_{\text{tot}} = 4 \text{ kPa}$ ⁷ or at $1200 < T \leq 1500^\circ\text{C}$, $p_{\text{tot}} \geq 40 \text{ kPa}$ ⁸. On the other hand, at $T = 1450^\circ\text{C}$, $p_{\text{tot}} = 1 \text{ kPa}$ or at $T > 1450^\circ\text{C}$, $p_{\text{tot}} \leq 10 \text{ kPa}$, highly $\langle 110 \rangle$ -oriented 3C-SiC was obtained⁸. Similarly, with C_3H_8 as carbon source, the growth at $T = 1200^\circ\text{C}$, $p_{\text{tot}} = 4 \text{ kPa}$, was highly $\langle 111 \rangle$ -oriented, but switches to $\langle 110 \rangle$ at elevated temperatures^{7,9}. No explanation for these changes in preferred growth orientation was suggested in these studies. Highly $\langle 111 \rangle$ -oriented 3C-SiC has also been prepared with hexamethyldisilane via laser

CVD^{10–14}. However, due to the small laser spot size, the coating area was limited to less than 20 x 20 mm.

Although it appears that small aliphatic hydrocarbons are favored in 3C-SiC CVD, presumably owing to their relatively simpler structures, the use of aromatics as carbon precursor in CVD of other metal carbides has been reported. Nagai et al. deposited β -Mo₂C thin films using benzene as carbon precursor¹⁵, whereas toluene was used for the deposition of SiC reported by Zhuravlov et al¹⁶. TiC_x was prepared both from benzene¹⁷ and toluene¹⁸. However, either amorphous carbon or pyrolytic graphite was detected in most of these carbide films. Despite the risk of carbon co-deposition, the use of aromatic hydrocarbons as carbon precursor may also influence the preferred growth orientation of deposited films. In the work of Leonhardt et al., a transition of preferred growth orientation from $\langle 100 \rangle$ to $\langle 111 \rangle$ with the change of carbon precursors from aliphatic, e.g. methane, to aromatic hydrocarbons, e.g. benzene, was observed in the growth of TiC_x. This phenomenon was later interpreted by Pedersen et al. through quantum chemical calculations where they claimed that the adsorption energy of benzene molecules on TiC(111) surfaces was higher than that on TiC(100), resulting in a $\langle 111 \rangle$ -oriented growth, whereas methane molecules did not exhibit preferential adsorption on either surfaces, and therefore the TiC would preferentially grow on the surface that has the lowest surface energy, i.e. (100) in TiC¹⁹. While both TiC and 3C-SiC are face-centered cubic crystal systems, TiC adopts the rock-salt structure, (B1, No. 225), and 3C-SiC the zincblende structure, (B3, No. 216). Despite their structural difference, the crystal plane along $\langle 111 \rangle$ direction in both crystals is terminated only with either C or Si/Ti atoms. This indicates that the (111) planes of TiC and 3C-SiC may exhibit similar properties for adsorbing molecules; therefore, the growth direction of 3C-SiC can possibly be steered in the same way as in the growth of TiC.

In this work, we test this hypothesis and demonstrated the possibility of controlling the preferred growth orientation of polycrystalline 3C-SiC between $\langle 111 \rangle$ and $\langle 110 \rangle$ by using either toluene or methane as carbon precursors in SiCl₄-based SiC CVD. Furthermore, by quantum chemical calculations we show how the adsorption behavior of benzene and methyl group differs when they approach the 3C-SiC (111) and (110) surfaces.

METHODS

Film deposition. 3C-SiC coatings were deposited on isostatic graphite substrates (100 mm x 60 mm x 1.5 mm) via a horizontal hot-wall chemical vapor deposition (CVD) reactor using silicon tetrachloride (SiCl_4) and either methane (CH_4) or toluene (C_7H_8). The liquid SiCl_4 and C_7H_8 were stored in stainless steel bubblers placed in a water bath whose temperature was maintained at 24.3 °C by a thermostat. The corresponding vapor pressure of SiCl_4 and C_7H_8 at this temperature is 30.7 kPa and 3.6 kPa, respectively. Hydrogen, purified by Ag-Pd alloy membranes, was utilized both as a diluting and carrier gas, directing the precursors from the bubblers to the reaction chamber. During the deposition, the substrate was situated in an inductively heated SiC-coated graphite susceptor. The temperature control within the reactor was realized by an optical pyrometer which measures the temperature through a view port. A throttle valve located between the chamber and the process pump regulated the pressure by adjusting its degree of opening. All 3C-SiC coatings in this study were prepared at a pressure of 10 kPa with a $p_{\text{C}}/p_{\text{Si}} = 1$ and a $p_{\text{H}_2}/p_{\text{Si}} = 23$ in the gas phase, at temperatures between 1100 °C and 1350 °C for the C_7H_8 process and between 1100 °C and 1400 °C for the CH_4 process.

Characterization. The 3C-SiC coated graphite plates were broken into 4 equal-sized pieces along the gas flow direction to probe the film deposition. The characterizations, i.e. X-ray diffraction (XRD), scanning electron microscopy (SEM) and Raman measurement, have been carried out mainly on the third piece from the inlet of the susceptor. The structure and phase of as-deposited samples was examined by XRD (PANalytical X'Pert PRO Powder X-ray Diffractometer) operating at a voltage of 45 kV and a current of 40 mA. The characteristic $\text{Cu-K}\alpha$ radiation with a wavelength of 1.54 Å was used to perform the $\theta/2\theta$ -scan between 20° and 140° in a Bragg-Brentano configuration with a divergence and an anti-scatter slit of 0.5°. A Ni filter was placed before the X'Celerator detector running in scanning line mode to remove $\text{Cu-K}\beta$ line. The resultant diffraction patterns were compared to the Powder Diffraction File (PDF) cards and the reflection peaks corresponding to certain lattice planes were assigned. The PDF cards that were referenced for 3C-SiC and graphite in this work are #00-029-1129 and #00-056-0159, respectively. The preferred growth orientation of the 3C-SiC coatings was quantified by the texture coefficient (TC)⁹ defined as follows:

$$TC_{(hkl)} = \frac{I_{m(hkl)}/I_{0(hkl)}}{(\frac{1}{n}) \sum [I_{m(hkl)}/I_{0(hkl)}]}$$

where (hkl) is the growth plane considered, I_m the normalized measured intensity (with the background intensity subtracted), I_0 the intensity of a randomly oriented polycrystalline sample (taken from the PDF card) and n the number of planes that are considered. Here, plane (111), (200), (220), (311), (222) and (331) were used for the TC calculation; therefore, n was equal to 6. The surface morphology and cross-section of the samples were probed by a field emission SEM (ZEISS LEO1550) using an acceleration voltage of 3 kV at a working distance around 5 mm. The existence of pyrolytic carbon in the coatings were investigated by a Raman spectrometer where Ar laser with a wavelength of 532 nm and a power of 10 mW was employed to excite the chemical bonds.

Computational methods. The adsorption behaviors of C_6H_6 and CH_3 molecules on 3C-SiC (111) and (110) planes were studied by quantum chemical calculation via the software Gaussian 16²⁰. The (111) and (110) surfaces are modeled using $Si_{15}C_{15}$ and $Si_{16}C_{16}$ clusters, respectively, both containing 4 atomic planes. To preserve the bulk structure of SiC, the lateral and bottom side of the clusters are saturated with hydrogen atoms. As for the top surface, the (111) plane is terminated with Si atoms without H-saturation, while on the (110) plane only C atoms are saturated with hydrogen. The geometries of these clusters are optimized by calculations based on density functional theory (DFT) using B3LYP functionals^{21,22} with the 6-31G(*d*, *p*) basis set and the empirical dispersion corrections D3 proposed by Grimme et al.²³ The spin configuration giving the lowest energy and the least distorted structure were used for each cluster. The adsorption energy, E_{ads} , is calculated as follows:

$$E_{ads} = E_{optimized\ geometry} - (E_{cluster} + E_{molecule}),$$

where $E_{cluster}$ and $E_{molecule}$ is the energy of bare surfaces and of molecules, e.g. C_6H_6 or CH_3 , in the gas phase, respectively, while $E_{optimized\ geometry}$ is the energy of the optimized structure including both adsorbate and adsorbent.

Results and Discussion

The use of C_7H_8 as the carbon source resulted in distinct surface morphologies and cross-sections as shown in Figure 1 and Figure 2, respectively. At a deposition temperature equal to or lower than $1250\text{ }^{\circ}\text{C}$, the growth is columnar, and the sample surface is dominated with the crystals resembling the top of hexagonal pyramids. It can also be noticed that the crystal size first increases when temperature rises from $1100\text{ }^{\circ}\text{C}$ to $1200\text{ }^{\circ}\text{C}$ and slightly decreases at $1250\text{ }^{\circ}\text{C}$. The 6-fold symmetric pyramids was assumed to be formed by a pair of twin triangular pyramids joining each other¹² and is a typical morphology of coatings with $\langle 111 \rangle$ -oriented face-centered cubic (FCC) crystal structure²⁴, whereas the pyramids with 4-fold symmetry was reported to be FCC crystals with $\langle 110 \rangle$ orientation²⁴. The dense and dark striations seen in either the surface morphologies (Figure 1) or the cross-sections (Figure 2) of the samples prepared at $T \leq 1250\text{ }^{\circ}\text{C}$ has previously been shown to be twins parallel to the (111) planes¹³, implying that these samples are highly $\langle 111 \rangle$ -oriented. When the temperature is further increased above $1300\text{ }^{\circ}\text{C}$, the surface turns into loose fibers and the coating becomes porous, suggesting a different deposition chemistry.

Figure 3(a) presents the θ - 2θ scan X-ray diffractograms of the coatings prepared with $SiCl_4$ and C_7H_8 at various temperatures. 3C-SiC is the major crystalline phase detected in most of the samples. At $T \leq 1250\text{ }^{\circ}\text{C}$, the samples are highly- $\langle 111 \rangle$ oriented because the diffractions from 3C-SiC (111), (222) and (333) planes, corresponding to 2θ of 35.6° , 75.5° and 133.4° , are almost the only peaks observed. At $T \geq 1300\text{ }^{\circ}\text{C}$, the intense peak from 3C-SiC (220) plane at $2\theta = 60.0^{\circ}$ indicates that the coatings are more $\langle 110 \rangle$ -oriented. At $T = 1350\text{ }^{\circ}\text{C}$, a rather weak graphite peak at $2\theta = 77.5^{\circ}$ from the substrate is also observed.

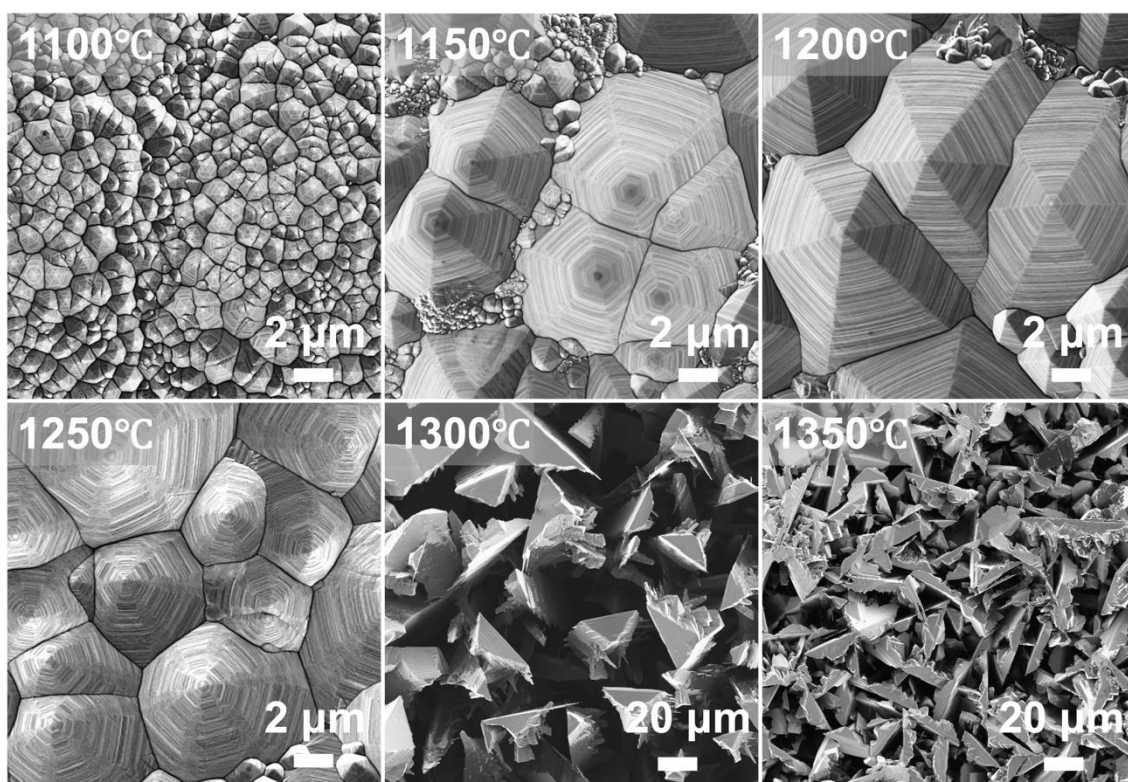


Figure 1. Surface morphologies of 3C-SiC coatings deposited with SiCl_4 and C_7H_8 at various temperatures

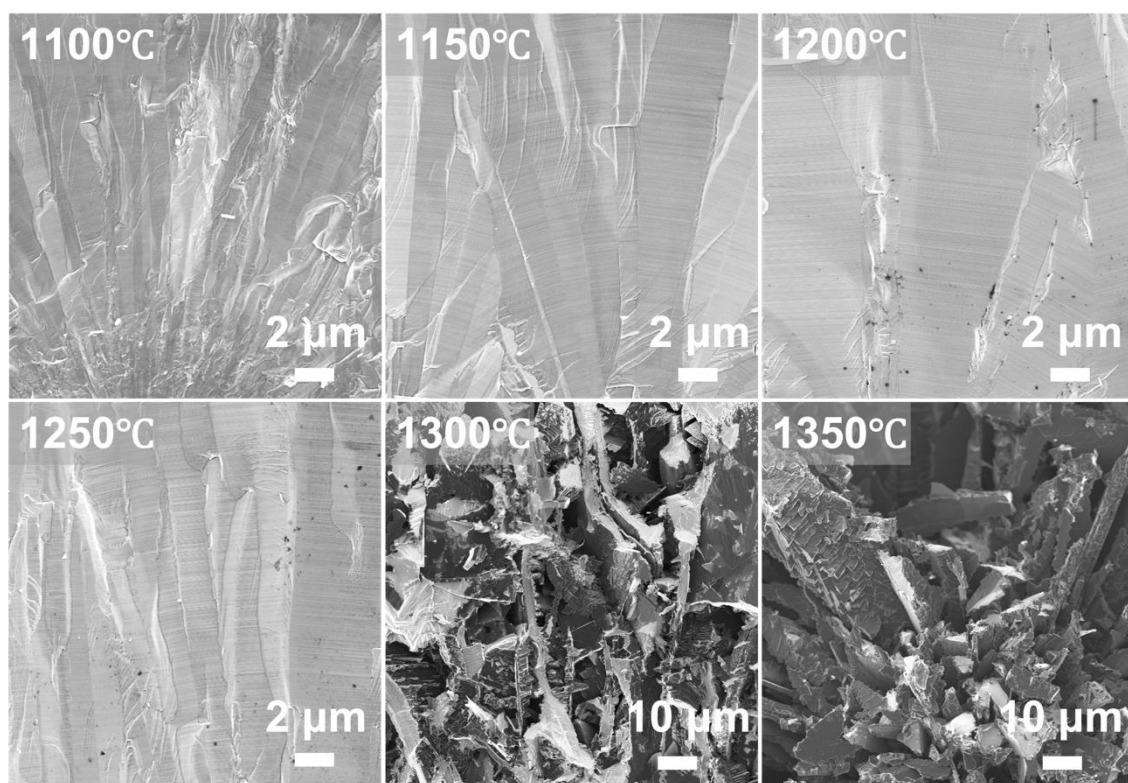


Figure 2. Cross sections of 3C-SiC coatings deposited with SiCl_4 and C_7H_8 at various temperatures

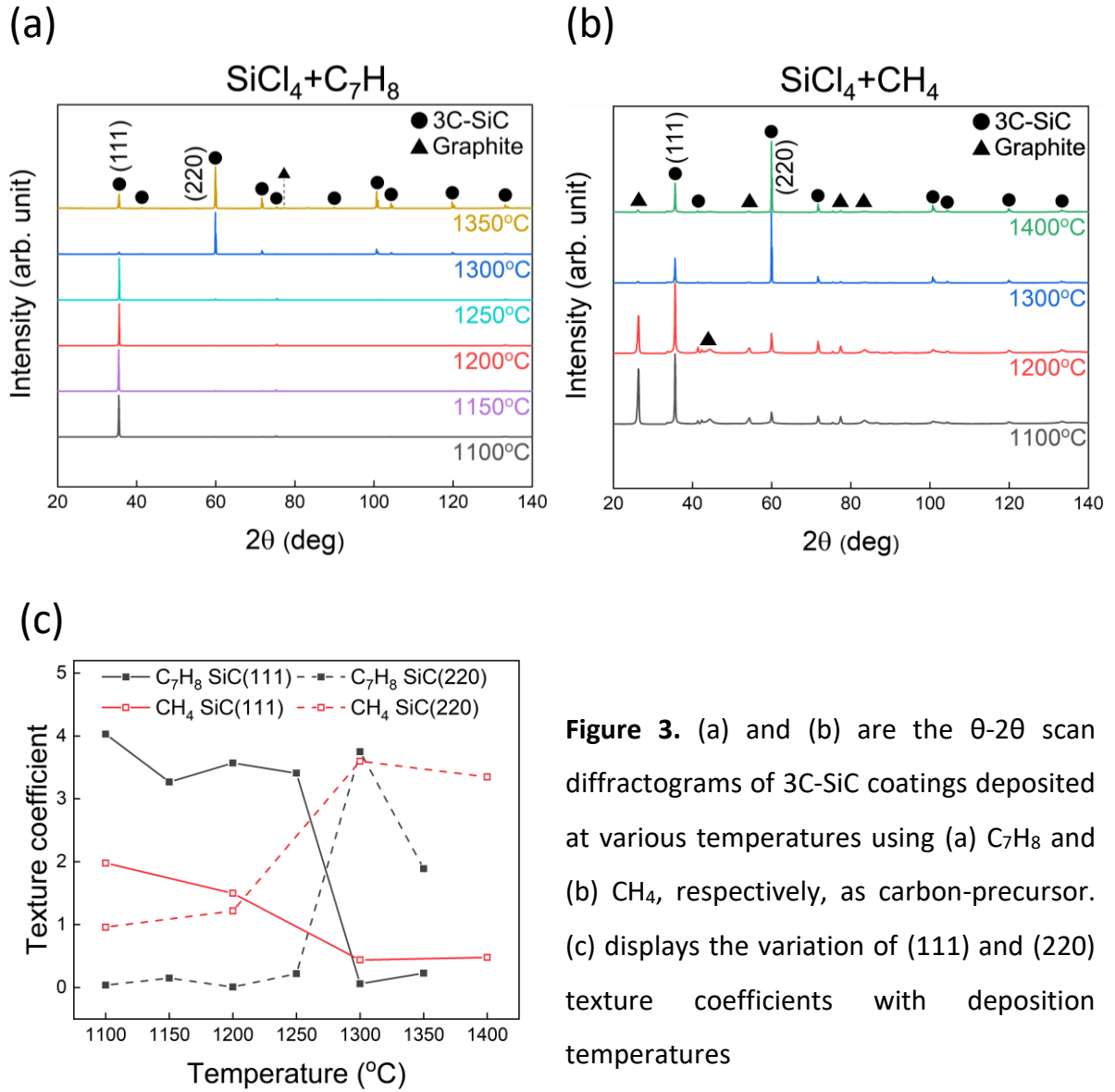


Figure 3. (a) and (b) are the θ - 2θ scan diffractograms of 3C-SiC coatings deposited at various temperatures using (a) C_7H_8 and (b) CH_4 , respectively, as carbon-precursor. (c) displays the variation of (111) and (220) texture coefficients with deposition temperatures

Under similar conditions, CH_4 has also been utilized for the growth of 3C-SiC coatings. The surface morphology, cross-sections and diffractograms of the deposited coatings are displayed in Figure 4, Figure 5 and Figure 3(b), respectively. At $T \leq 1200^\circ\text{C}$, the surface resembles cauliflowers with small, non-faceted SiC crystallites, whereas at $T > 1200^\circ\text{C}$ faceted crystals which increase in size with increasing deposition temperature are formed. A growth mode transition from fine crystallite to columnar with increasing temperature can be observed in the cross-sectional images shown in Figure 5. In contrast to the C_7H_8 process where a shift of growth orientation from $\langle 111 \rangle$ to $\langle 110 \rangle$ is seen with higher temperatures, the diffractograms for the 3C-SiC coatings prepared in the CH_4 process show a change from randomly oriented to $\langle 110 \rangle$ -oriented growth between 1200°C and 1300°C .

In Figure 3(c) the quantified growth orientation, i.e., the texture coefficient (TC), of 3C-SiC coatings deposited with C_7H_8 and CH_4 is plotted versus the deposition temperature. (111) and (110) planes of 3C-SiC are chosen for comparison because they are the first and second strongest reflections in the diffractogram of randomly oriented polycrystalline 3C-SiC powder. For both C_7H_8 and CH_4 processes, a transition of growth orientation can be observed. At higher temperatures (C_7H_8 : $T \geq 1300\text{ }^{\circ}\text{C}$, CH_4 : $T > 1200\text{ }^{\circ}\text{C}$), the 3C-SiC coatings from both processes are highly $\langle 110 \rangle$ -oriented. At lower temperatures (C_7H_8 : $T \leq 1250\text{ }^{\circ}\text{C}$, CH_4 : $T < 1200\text{ }^{\circ}\text{C}$), 3C-SiC coatings deposited with CH_4 exhibit no strongly preferred growth orientation, whereas the ones prepared with C_7H_8 are highly $\langle 111 \rangle$ -oriented. These observations are in accord with the change in surface morphology seen in the SEM images. Because the deposition conditions in both sets of experiments were similar except for the used hydrocarbon, it is inferred that the difference in growth orientation at low temperature is caused by the choice of hydrocarbon.

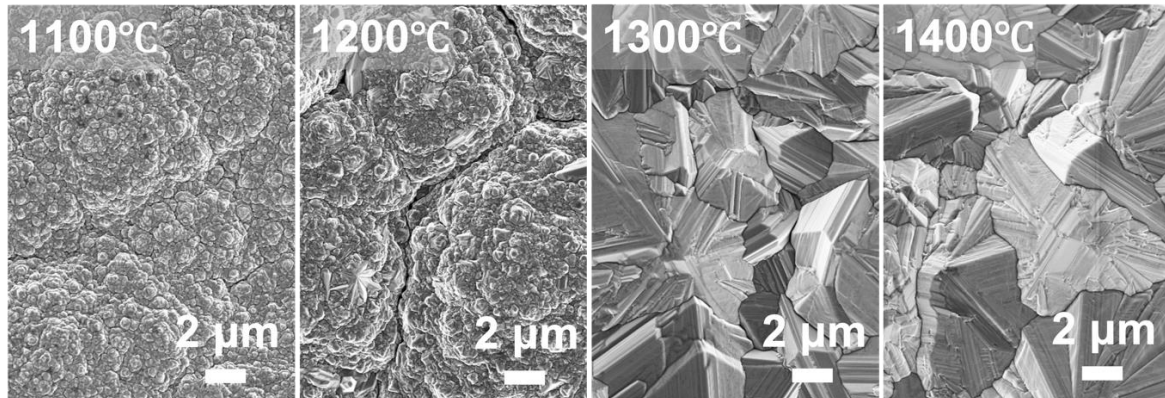


Figure 4. Surface morphologies of 3C-SiC coatings deposited with $SiCl_4$ and CH_4 at various temperatures

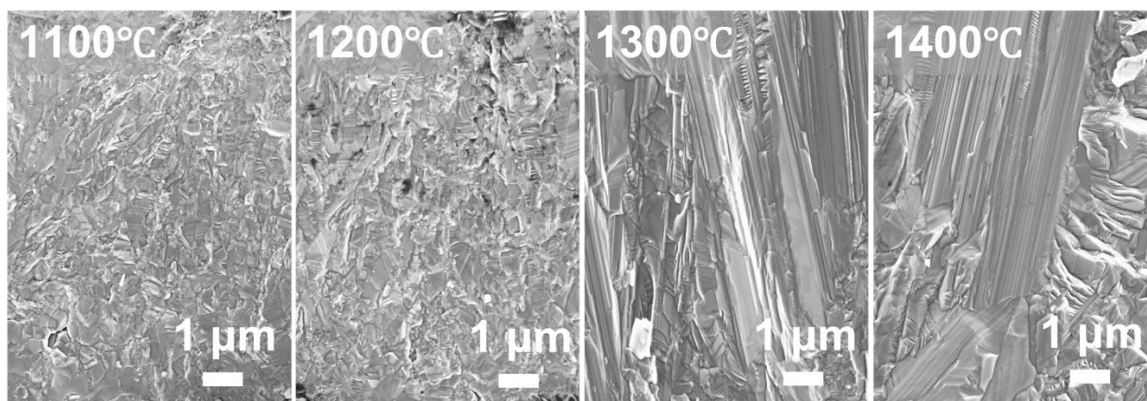


Figure 5. Cross sections of 3C-SiC coatings deposited with SiCl_4 and CH_4 at various temperatures

In order to investigate whether the use of aromatic hydrocarbons would result in the formation of excess carbon in the films, the Raman measurements have been performed on the 3C-SiC coatings deposited either with CH_4 or C_7H_8 as shown in Figure 6. In the CH_4 process, the Raman spectra of deposited 3C-SiC coatings shows a Raman shift deviation of $\pm 1 \text{ cm}^{-1}$ in both 1st order 3C-SiC transverse optical (TO) and longitudinal optical (LO) mode. The Raman shifts for 1st order TO and MO modes of bulk 3C-SiC are reported to be 796 cm^{-1} and 972 cm^{-1} , respectively²⁵. On the other hand, an even higher deviation of Raman shift for 1st order TO and MO modes is observed in the 3C-SiC coatings prepared with C_7H_8 with the corresponding TO at $794 \pm 2 \text{ cm}^{-1}$ and LO at $967 \pm 2 \text{ cm}^{-1}$. The 2nd order TO and LO modes of 3C-SiC²⁶ at 1520 cm^{-1} and 1710 cm^{-1} , respectively, are also detected in both processes. Moreover, at lower temperatures (C_7H_8 : $T < 1200 \text{ }^\circ\text{C}$, CH_4 : $T \leq 1200 \text{ }^\circ\text{C}$), broadened transverse acoustic (TA) and longitudinal acoustic (LA) modes of 3C-SiC, which are normally located between 150 and 600 cm^{-1} , are observed, indicating the existence of smaller SiC crystallites^{27–29}. However, at $T \geq 1300 \text{ }^\circ\text{C}$, the characteristic Raman modes for carbon phases, e.g. D-band at 1350 cm^{-1} , G-band at 1580 cm^{-1} and 2D band at 2701 cm^{-1} ²⁷, are observed in the 3C-SiC samples prepared with C_7H_8 , indicating the co-deposition of pyrolytic carbon. It is noteworthy that the appearance of these Raman peaks is observed at the same temperature as the shift from $\langle 111 \rangle$ to $\langle 110 \rangle$ oriented growth. This could be caused by the breakdown of the toluene molecules forming highly reactive intermediates at such high temperatures. It could also be possible that the Si precursor is depleted faster than the C precursor, leaving excess carbon species in the coating. Either way, the presence of pyrolytic carbon indicates a change in the growth chemistry, which could be the cause of the change in crystalline orientation and morphology as seen in

SEM and XRD. Interestingly, no signs of pyrolytic carbon can be found in the coatings grown from CH_4 , even at high temperatures. A possible explanation is the different decomposition products of the hydrocarbons. Toluene will decompose into larger hydrocarbons that may more easily form condensed deposits, while CH_4 will only break down into even smaller radicals, which are less prone to form condensed pyrolytic carbon deposits.

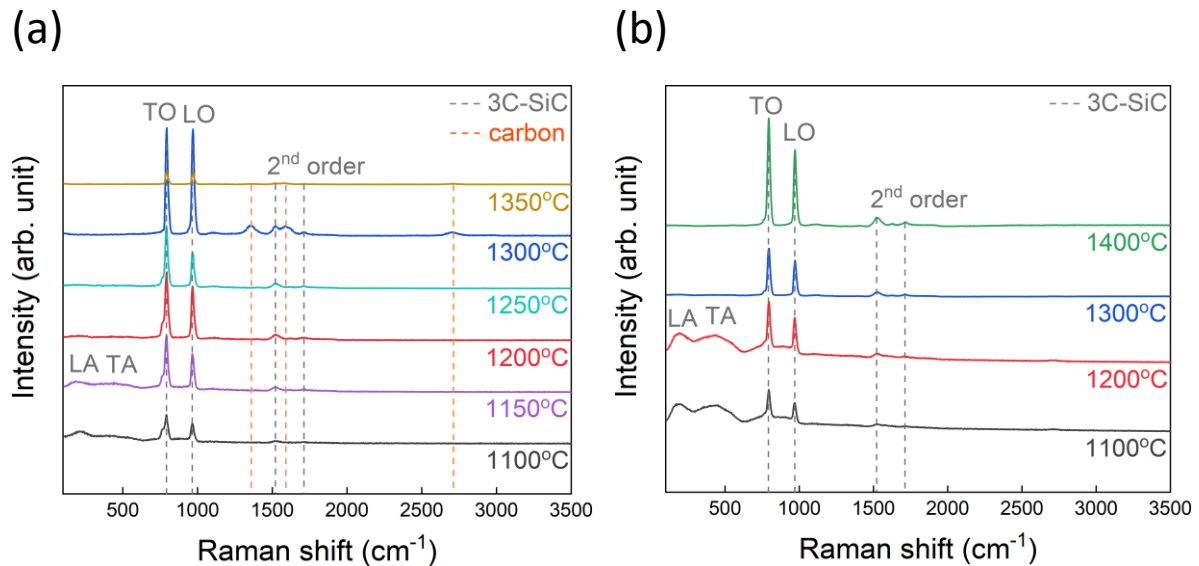


Figure 6. Raman spectra of 3C-SiC deposited at various temperatures using SiCl_4 as the Si precursor and **(a)** C_7H_8 and **(b)** CH_4 as carbon precursor.

The different growth regimes in the C_7H_8 process can also be observed in the Arrhenius plot displayed in Figure 7. From the data, there seems to be three growth regimes in the C_7H_8 process. For $T \leq 1250^\circ\text{C}$, the Arrhenius plot suggests that the growth is kinetically limited with an activation energy of 103 kJ/mol. At $1250^\circ\text{C} < T < 1300^\circ\text{C}$, the kinetics-controlled growth seems to retain but with a much higher activation energy. In this temperature range, the preferred growth orientation of 3C-SiC deposited with toluene switches from $\langle 111 \rangle$ to $\langle 110 \rangle$ direction and free carbon also starts to be incorporated into the films. The change of the slope in the Arrhenius plot and in the preferred growth orientation can be interpreted as an indication of change in the deposition chemistry. It should be noted that a change in deposition chemistry can also result in a change in reaction order, meaning that, e.g. the rate constant in the Arrhenius equation is not the same over the entire investigated temperature range in Figure. 7. When the temperature continues to rise above 1300°C , the deposition again alters its character, and the films grow in the form of more flake-like crystals (Figure 1).

This alteration is represented by a plateau in Figure 7, suggesting that at $T \geq 1300$ °C the deposition chemistry enters the mass-transport limited regime with an apparent activation energy of 5 kJ/mol. On the other hand, the 3C-SiC growth in the CH_4 process appears to be kinetics limited with an activation energy of 85 kJ/mol between 1100 °C and 1400 °C and the preferred growth orientation changes from randomly oriented to highly $\langle 110 \rangle$ at $T > 1200$ °C.

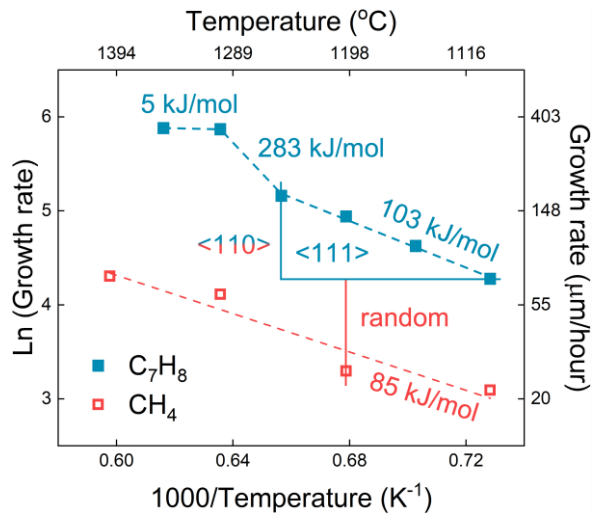
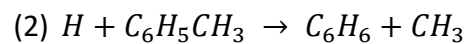
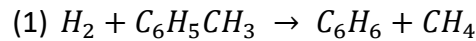


Figure 7. Arrhenius plot for SiCl_4 based 3C-SiC coatings using either CH_4 or C_7H_8 as carbon precursor. The data points from both processes are fitted with dashed lines.

To further understand the deposition chemistry, the adsorption behaviors of C_6H_6 and CH_3 on the 3C-SiC (111) and (110) planes are studied by DFT calculations. A toluene molecule consists of a benzene ring (C_6H_6) with one of its H atoms replaced by a methyl group (CH_3), whereas a methane molecule is composed of four equivalent C-H bonds forming a tetrahedron. In an environment with large excess of hydrogen and at elevated temperatures, toluene was reported to undergo two possible decomposition pathways^{30,31}:



CH_4 does not directly contribute towards the SiC growth³², but only via the decomposition into CH_3 . The active carbon species for the adsorption studies are thus considered to be C_6H_6 and CH_3 species. Figure 8 presents the calculation results for the adsorption of the abovementioned two molecules on 3C-SiC (111) and (110) planes. It can be noticed that CH_3 is easily adsorbed on both planes and the adsorption energy on (111) and (110) is calculated to be -376 kJ/mol and -368 kJ/mol, respectively. Moreover, the distance between the C atom

from the CH₃ and the surface Si atom was reduced from the initial 2 Å position to 1.89 Å [(111) plane] and 1.90 Å [(110) plane] after adsorption, which is comparable to the C-H bond length in bulk 3C-SiC. The result suggests that the CH₃ does not show a strong preference towards the (111) or (110) plane, since the adsorption energies of CH₃ on both planes are very close to each other. The C₆H₆ molecule is also active towards the (111) plane, exhibiting an adsorption energy of –278 kJ/mol. Upon adsorption, the C₆H₆ molecule loses its planar symmetry: three C atoms of the molecule move away from the (111) surface, and the other three move down towards the (111) surface. The distance between the three C atoms closest to the surface and the surface Si atoms are decreased to 1.95±0.01 Å. However, the C₆H₆ molecule seems to be rather inactive towards (110) plane, the distance between which after calculation increased from 2 Å to 3.54 Å corresponding to an adsorption energy of –46 kJ/mol. Judging from the adsorption energy and the distance between adsorbate and surface, the C₆H₆ molecule is considered physisorbed on the (110) plane, whereas the adsorption of C₆H₆ on (111) as well as that of CH₃ on both (111) and (110) can be described as chemisorption which would lead to the formation of chemical bonding.

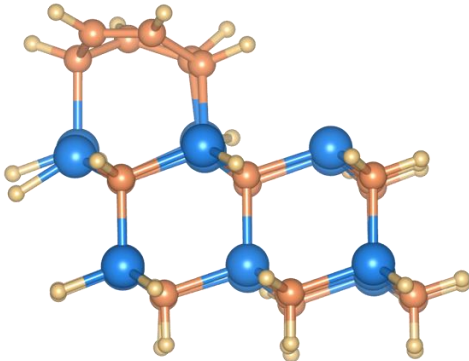
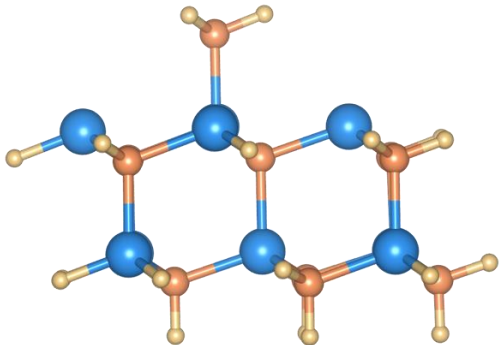
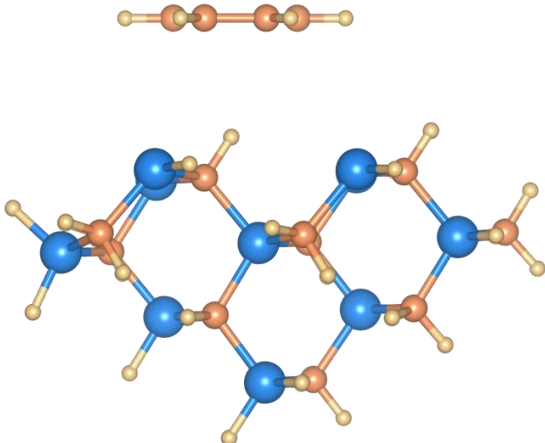
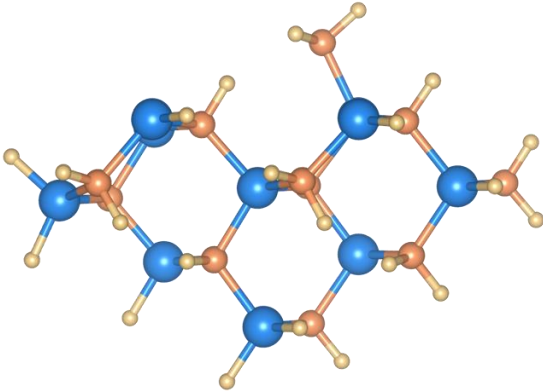
	C ₆ H ₆	CH ₃
3C-SiC (111)	 $E_{\text{ads}} = -278 \text{ kJ/mol}, S = 4$	 $E_{\text{ads}} = -376 \text{ kJ/mol}, S = 7$
3C-SiC (110)	 $E_{\text{ads}} = -46 \text{ kJ/mol}, S = 7$	 $E_{\text{ads}} = -368 \text{ kJ/mol}, S = 6$

Figure 8. Computational results of the adsorption of C₆H₆ and CH₃ on 3C-SiC (111) and (110) planes and their corresponding adsorption energies, E_{ads} . S denotes the spin configuration that yielded the lowest energy and the least distorted structure after calculation

The SiC crystals in the films are expected to grow along the atomic direction whose corresponding atomic plane has the lowest surface energy. According to Kikuchi et al., the surface energy of the first three low index 3C-SiC planes, namely, (100), (111) and (110), is 6.8 J/m², 4.2 J/m² and 3.4 J/m², respectively⁶. This implies that in the conventional 3C-SiC CVD most of the coatings would grow preferentially along <110> direction. When we use CH₄ at 1100 - 1400 °C we observe a random or <110>-preferred growth direction. By using C₇H₈ as

carbon precursor instead, it was possible to deposit highly $\langle 111 \rangle$ -oriented 3C-SiC coatings at $T \leq 1250$ °C. This change of preferred growth orientation with aromatic hydrocarbons was previously observed for the CVD growth of TiC hard coatings.¹⁷ For TiC, this was suggested to be due to the stronger adsorption of C_6H_6 on the (111) surface compared to the (100) surface, overcoming the lower surface energy of the (100) surface.¹⁹ Based on the reported CVD chemistry for toluene^{30,31}, the active carbon-containing growth species in the C_7H_8 process are assumed to be C_6H_6 and CH_3 , whereas in the CH_4 process CH_3 is supposed to be the active species.³³ As described above, the computational results showed that CH_3 was chemisorbed on both 3C-SiC (111) and (110) planes, and C_6H_6 was chemisorbed on the (111) plane but physisorbed on the (110) plane. The slight difference in the adsorption energies of CH_3 on both (111) and (110) explains the almost randomly oriented SiC growth in the CH_4 process. On the other hand, the highly- $\langle 111 \rangle$ oriented 3C-SiC coatings prepared using C_7H_8 can be assumed to result from the significant adsorption energy difference of C_6H_6 on (111) and (110) planes. The energy decrease resulting from the adsorption of C_6H_6 on the (111) plane is 6 times larger than that on (110). At higher temperatures, toluene is expected to decompose into various hydrocarbons³⁴, and therefore the growth of 3C-SiC is no longer directed towards the $\langle 111 \rangle$ direction. Without the directing effect of the aromatic hydrocarbon, the growth happens mainly on the (110) planes having the lowest surface energy, which is similar to the case in the CH_4 process.

Conclusion

In this work, we were able to control the preferred growth orientation of 3C-SiC by using either methane (CH_4) or toluene (C_7H_8) as the carbon precursor in a $SiCl_4$ -based SiC CVD. At $T \leq 1250$ °C and $p = 10$ kPa, the resulting 3C-SiC coatings were highly $\langle 111 \rangle$ -oriented in the C_7H_8 process, whereas they were almost randomly oriented in the CH_4 process. At $T > 1250$ °C both processes resulted in highly $\langle 110 \rangle$ -oriented 3C-SiC coatings. By considering C_6H_6 and CH_3 the main active carbon-containing film forming species, their adsorption behaviors on 3C-SiC (111) and (110) planes were shown via quantum chemical calculation to be significantly different: C_6H_6 was chemisorbed on the (111) plane, but physisorbed on the (110) plane, while CH_3 was chemisorbed strongly on both planes. These calculation results indicate that the difference in reactivity of the carbon precursor towards the various planes is the reason for

the different growth orientations. At $T > 1250\text{ }^{\circ}\text{C}$, the transition to highly $\langle 110 \rangle$ -oriented growth in both processes can be explained by the fact that 3C-SiC would tend to grow along the direction leading to the lowest surface energy, i.e. (110) plane in 3C-SiC. The steering effect of toluene is no longer present at elevated temperatures due to its expected decomposition into smaller, non-aromatic hydrocarbons.

Acknowledgement

The authors thank SGL CARBON GmbH for the financial support. L. Ojamäe acknowledges support from the Swedish Research Council (VR). Rickard Liljedahl is acknowledged for fruitful discussions and for the support in sample characterizations.

Reference

- (1) Choy, K. Chemical Vapour Deposition of Coatings. *Progress in Materials Science* **2003**, 48 (2), 57–170. [https://doi.org/10.1016/S0079-6425\(01\)00009-3](https://doi.org/10.1016/S0079-6425(01)00009-3).
- (2) Pedersen, H.; Leone, S.; Kordina, O.; Henry, A.; Nishizawa, S.; Koshka, Y.; Janzén, E. Chloride-Based CVD Growth of Silicon Carbide for Electronic Applications. *Chem. Rev.* **2012**, 112 (4), 2434–2453. <https://doi.org/10.1021/cr200257z>.
- (3) Aylward, G.; Findlay, T. *SI Chemical Data*, 4th ed.; John Wiley & Sons, 1999.
- (4) Yazdanfar, M.; Danielsson, Ö.; Kordina, O.; Janzén, E.; Pedersen, H. Finding the Optimum Chloride-Based Chemistry for Chemical Vapor Deposition of SiC. *ECS J. Solid State Sci. Technol.* **2014**, 3 (10), P320–P323. <https://doi.org/10.1149/2.0111410jss>.
- (5) Kim, H.-S.; Choi, D.-J. The Reactant Depletion Effect on Chemically Vapor Deposited SiC Films with Pressure and Gas Ambient. *Thin Solid Films* **1998**, 312 (1–2), 195–201. [https://doi.org/10.1016/S0040-6090\(97\)00744-X](https://doi.org/10.1016/S0040-6090(97)00744-X).
- (6) Kikuchi, H.; Kalia, R. K.; Nakano, A.; Vashishta, P.; Branicio, P. S.; Shimojo, F. Brittle Dynamic Fracture of Crystalline Cubic Silicon Carbide (3C-SiC) via Molecular Dynamics Simulation. *Journal of Applied Physics* **2005**, 98 (10), 103524. <https://doi.org/10.1063/1.2135896>.
- (7) Tu, R.; Zheng, D. H.; Cheng, H.; Han, M. X.; Zhang, S.; Goto, T. Preparation of Ultra-Thick β -SiC Films Using Different Carbon Sources. *Materials Research Innovations* **2015**, 19 (sup10), S10-397-S10-402. <https://doi.org/10.1179/1432891715Z.00000000002205>.
- (8) Tu, R.; Zheng, D.; Sun, Q.; Han, M.; Zhang, S.; Hu, Z.; Goto, T.; Zhang, L. Ultra-Fast Fabrication of $\langle 110 \rangle$ -Oriented β -SiC Wafers by Halide CVD. *J. Am. Ceram. Soc.* **2016**, 99 (1), 84–88. <https://doi.org/10.1111/jace.13980>.
- (9) Lin, T. T.; Hon, M. H. The Growth Characteristics of Chemical Vapour-Deposited β -SiC on a Graphite Substrate by the $\text{SiCl}_4/\text{C}_3\text{H}_8/\text{H}_2$ System. *Journal of Materials Science* **1995**, 30 (10), 2675–2681. <https://doi.org/10.1007/bf00362151>.
- (10) Xu, Q.; Zhu, P.; Sun, Q.; Tu, R.; Zhang, S.; Yang, M.; Li, Q.; Shi, J.; Li, H.; Zhang, L.; Goto, T.; Han, M.; Yan, J.; Li, S.; Ohmori, H. Fast Preparation of $\langle 111 \rangle$ -Oriented β -SiC Films without Carbon Formation by Laser Chemical Vapor Deposition from Hexamethyldisilane without H_2 . *J Am Ceram Soc* **2018**, 101 (4), 1471–1478. <https://doi.org/10.1111/jace.15315>.
- (11) Zhu, P. P.; Tu, R.; Zhang, S.; Han, M. X.; Xu, Q. F.; Sun, Q. Y.; Zhang, L. M.; Goto, T.; Yan, J. S.; Li, S. S. The Effect of Diluent Gases on the Growth of β -SiC Films by Laser CVD with HMDS. *Materials Research Innovations* **2015**, 19 (sup10), S10-403-S10-407. <https://doi.org/10.1179/1432891715Z.00000000002208>.
- (12) Zhang, S.; Xu, Q.; Sun, Q.; Zhu, P.; Tu, R.; Hu, Z.; Han, M.; Goto, T.; Zhang, L.; Yan, J.; Li, S. Effect of Pressure on Microstructure of $\langle 111 \rangle$ -Oriented β -SiC Films: Research via Electron Backscatter Diffraction. *J. Am. Ceram. Soc.* **2015**, 98 (12), 3713–3718. <https://doi.org/10.1111/jace.13823>.
- (13) Zhang, S.; Xu, Q.; Tu, R.; Goto, T.; Zhang, L. High-Speed Preparation of $\langle 111 \rangle$ - and $\langle 110 \rangle$ -Oriented β -SiC Films by Laser Chemical Vapor Deposition. *J. Am. Ceram. Soc.* **2014**, 97 (3), 952–958. <https://doi.org/10.1111/jace.12706>.
- (14) Zhang, S.; Xu, Q.; Tu, R.; Goto, T.; Zhang, L. Growth Mechanism and Defects of $\langle 111 \rangle$ -Oriented β -SiC Films Deposited by Laser Chemical Vapor Deposition. *J. Am. Ceram. Soc.* **2015**, 98 (1), 236–241. <https://doi.org/10.1111/jace.13248>.

- (15) Nagai, M.; Shishikura, I.; Omi, S. Molybdenum Carbide Prepared by Chemical Vapor Deposition. *Jpn. J. Appl. Phys.* **2000**, 39 (Part 1, No. 7B), 4528–4531. <https://doi.org/10.1143/JJAP.39.4528>.
- (16) Zhuravlov, A. Yu.; Hovanskiy, N. A.; Khizhnyak, D. A.; Shirokov, B. M.; Semenov, N. A.; Shijan, A. V.; Strigunovskiy, S. V.; Yevsiukov, A. I.; Shevtsov, A. B.; Nazarenko, E. A.; Pilipenko, N. N. Obtaining Silicon Carbide via Chemical Vapor, Plasma-Chemical and Sublimation Methods. *Problems of Atomic Science and Technology* **2017**.
- (17) Leonhardt, A.; Wolf, E. Influence of Different Hydrocarbons on the Structure of CVD- and PACVD-TiCx Hard Layers. *Materials Science and Engineering: A* **1996**, 209 (1–2), 389–393. [https://doi.org/10.1016/0921-5093\(95\)10110-1](https://doi.org/10.1016/0921-5093(95)10110-1).
- (18) López-Romero, S.; Chávez-Ramírez, J. Synthesis of TiC Thin Films by CVD from Toluene and Titanium Tetrachloride with Nickel as Catalyst. *Matéria (Rio de Janeiro)* **2007**, 12 (3), 487–493. <https://doi.org/10.1590/s1517-70762007000300009>.
- (19) Pedersen, H.; Lin, C.-C.; Ojamäe, L. On the Change of Preferential Growth Orientation in Chemical Vapor Deposition of Titanium Carbide by Aromatic Hydrocarbon Precursors. *Journal of Vacuum Science & Technology A: Vacuum, Surfaces, and Films* **2013**, 31 (2), 021507. <https://doi.org/10.1116/1.4792723>.
- (20) M. J. Frisch, G. W. Trucks, H. B. Schlegel, G. E. Scuseria,; M. A. Robb, J. R. Cheeseman, G. Scalmani, V. Barone,; G. A. Petersson, H. Nakatsuji, X. Li, M. Caricato, A. V. Marenich,; J. Bloino, B. G. Janesko, R. Gomperts, B. Mennucci, H. P. Hratchian,; J. V. Ortiz, A. F. Izmaylov, J. L. Sonnenberg, D. Williams-Young,; F. Ding, F. Lipparini, F. Egidi, J. Goings, B. Peng, A. Petrone,; T. Henderson, D. Ranasinghe, V. G. Zakrzewski, J. Gao, N. Rega,; G. Zheng, W. Liang, M. Hada, M. Ehara, K. Toyota, R. Fukuda,; J. Hasegawa, M. Ishida, T. Nakajima, Y. Honda, O. Kitao, H. Nakai,; T. Vreven, K. Throssell, J. A. Montgomery, Jr., J. E. Peralta,; F. Ogliaro, M. J. Bearpark, J. J. Heyd, E. N. Brothers, K. N. Kudin,; V. N. Staroverov, T. A. Keith, R. Kobayashi, J. Normand,; K. Raghavachari, A. P. Rendell, J. C. Burant, S. S. Iyengar,; J. Tomasi, M. Cossi, J. M. Millam, M. Klene, C. Adamo, R. Cammi,; J. W. Ochterski, R. L. Martin, K. Morokuma, O. Farkas,; J. B. Foresman, and D. J. Fox. *Gaussian 16, Revision C.01*; Gaussian, Inc.: Wallingford CT, 2019.
- (21) Becke, A. D. Density-functional Thermochemistry. III. The Role of Exact Exchange. *The Journal of Chemical Physics* **1993**, 98 (7), 5648–5652. <https://doi.org/10.1063/1.464913>.
- (22) Lee, C.; Yang, W.; Parr, R. G. Development of the Colle-Salvetti Correlation-Energy Formula into a Functional of the Electron Density. *Phys. Rev. B* **1988**, 37 (2), 785–789. <https://doi.org/10.1103/PhysRevB.37.785>.
- (23) Grimme, S.; Antony, J.; Ehrlich, S.; Krieg, H. A Consistent and Accurate Ab Initio Parametrization of Density Functional Dispersion Correction (DFT-D) for the 94 Elements H-Pu. *The Journal of Chemical Physics* **2010**, 132 (15), 154104. <https://doi.org/10.1063/1.3382344>.
- (24) Tu, R.; Zheng, D.; Cheng, H.; Hu, M.; Zhang, S.; Han, M.; Goto, T.; Zhang, L. Effect of CH₄/SiCl₄ Ratio on the Composition and Microstructure of <110>-Oriented β-SiC Bulks by Halide CVD. *Journal of the European Ceramic Society* **2017**, 37 (4), 1217–1223. <https://doi.org/10.1016/j.jeurceramsoc.2016.11.015>.
- (25) Feldman, D. W.; Parker, J. H.; Choyke, W. J.; Patrick, L. Phonon Dispersion Curves by Raman Scattering in SiC, Polytypes 3C,4H,6H,15R, and 21R. *Phys. Rev.* **1968**, 173 (3), 787–793. <https://doi.org/10.1103/PhysRev.173.787>.

- (26) Feng, Z. C.; Tin, C. C.; Hu, R.; Williams, J. Raman and Rutherford Backscattering Analyses of Cubic SiC Thin Films Grown on Si by Vertical Chemical Vapor Deposition. *Thin Solid Films* **1995**, *266* (1), 1–7. [https://doi.org/10.1016/0040-6090\(95\)06599-7](https://doi.org/10.1016/0040-6090(95)06599-7).
- (27) Dasgupta, A.; Klein, S.; Houben, L.; Carius, R.; Finger, F.; Luysberg, M. Microstructure of Highly Crystalline Silicon Carbide Thin Films Grown by HWCVD Technique. *Thin Solid Films* **2008**, *516* (5), 618–621. <https://doi.org/10.1016/j.tsf.2007.06.055>.
- (28) Dasgupta, A.; Huang, Y.; Houben, L.; Klein, S.; Finger, F.; Carius, R.; Luysberg, M. Effect of Filament and Substrate Temperatures on the Structural and Electrical Properties of SiC Thin Films Grown by the HWCVD Technique. *Thin Solid Films* **2008**, *516* (5), 622–625. <https://doi.org/10.1016/j.tsf.2007.06.077>.
- (29) Ward, Y.; Young, R. J.; Shatwell, R. A. A Microstructural Study of Silicon Carbide Fibres through the Use of Raman Microscopy. **2001**, 12.
- (30) Amano, A.; Tominaga, H.; Tokuhisa, H. Mechanism of Thermal Hydrogenolysis of Toluene. *Bull. Japan Petrol. Inst.* **1965**, *7*, 59–63. <https://doi.org/10.1627/jpi1959.7.59>.
- (31) Amano, A.; Horie, O.; Hanh, N. H. Effect of Thermal Activation on the Reaction of Toluene with Hydrogen Atoms. *Int. J. Chem. Kinet.* **1976**, *8* (3), 321–339. <https://doi.org/10.1002/kin.550080302>.
- (32) Sukkaew, P.; Danielsson, Ö.; Kordina, O.; Janzén, E.; Ojamäe, L. Ab Initio Study of Growth Mechanism of 4H–SiC: Adsorption and Surface Reaction of C₂H₂, C₂H₄, CH₄, and CH₃. *J. Phys. Chem. C* **2017**, *121* (2), 1249–1256. <https://doi.org/10.1021/acs.jpcc.6b11085>.
- (33) Stenberg, P.; Danielsson, Ö.; Erdtman, E.; Sukkaew, P.; Ojamäe, L.; Janzén, E.; Pedersen, H. Matching Precursor Kinetics to Afford a More Robust CVD Chemistry: A Case Study of the C Chemistry for Silicon Carbide Using SiF₄ as Si Precursor. *J. Mater. Chem. C* **2017**, *5* (23), 5818–5823. <https://doi.org/10.1039/C7TC00138J>.
- (34) Derudi, M.; Polino, D.; Cavallotti, C. Toluene and Benzyl Decomposition Mechanisms: Elementary Reactions and Kinetic Simulations. *Phys. Chem. Chem. Phys.* **2011**, *13* (48), 21308. <https://doi.org/10.1039/c1cp22601k>.